Research on Influence of Motor Parameters on the Negative-Salient Permanent Magnet Synchronous Motor

Fei Guo, Qiu Chu, Chunyan Li, and Tao Meng, *Member, IEEE*

***Abstract*—The d-axis inductance (L_d) of the negative-salient permanent magnet synchronous motor (NSPMSM) is larger than the q-axis inductance (L_q). Compared with the traditional motor, the NSPMSM has the characteristics of a high overload capacity, wide speed range, and preventing permanent magnet demagnetization. Positive d-axis current (i_d) is applied to control positive reluctance torque when running at base speed. When the motor is running at high speed, a relatively small i_d can achieve speed expansion and effectively expand the motor flux-weakening range. The use of a magnetic bridge to increase the L_d and a W-type permanent magnet to reduce the L_q is proposed in this article as a novel NSPMSM rotor structure. Firstly, the working principle of the NSPMSM was determined according to the equivalent magnetic circuit. Secondly, using the finite element method, the influence of motor structure on torque and speed performance of NSPMSM was analyzed, and the motor structure was optimized. Thirdly, the effect of the internal power factor angle on the performance of the two motors is analyzed. Finally, the short circuit simulation and analysis verified that the NSPMSM has a stronger short circuit current suppression ability without sacrificing overload ability.**

***Index Terms*—Speed range, inner power factor angle, flux weakening, torque, short-circuit current.**

I. Introduction

THE permanent magnet synchronous motor (PMSM) has been extensively researched and implemented in numerical control machine systems and other domains due to its advantages of small size and high efficiency [1]-[3]. The permanent magnet (PM) design of the W-type PMSM is flexible. Choosing the appropriate length and width of a W-type PM can effectively improve the magnetic flux of each pole of the motor, thus improving the output torque, and giving full play to the advantages of the high power density of PMSM. [4], [5]. PMSM is excited by the PM, and the fixed excitation source makes adjusting the magnetic field difficult, limiting its application in the field of speed regulation [6], [7]. There are two traditional flux-weakening methods: one is increasing the d-axis demagnetization current; the other is improving the d-axis inductance (L_d) [8]-[10]. When the armature current is constant, increasing the negative i_d will reduce the i_q, which will reduce the permanent magnet torque and may cause irreversible demagnetization. Increasing the L_d is limited by the structure of the motor. This is the reason why the traditional positive permanent magnet synchronous motor (PSPMSM) is difficult to weaken the magnetic field. Through the design of the PM structure of negative-salient permanent magnet synchronous motor (NSPMSM), the L_d is larger than the q-axis inductance (L_q). The NSPMSM has a larger L_d, which is more conducive to the realization of flux weakening. Therefore, the NSPMSM has become one of the research hot spots in the domains of PMSM and has been attracted extensive attention from scholars [11], [12].

In [13], the PM adopts a V-type segmented structure, which increases the L_d and reduces the eddy current loss of the PM. Part of the demagnetization magnetic field lines pass through the magnetic bridge during the flux-weakening state, improving the working point of the motor and facilitating the speed expansion of the flux-weakening state. In [14], [15], the arc magnetic barrier is set parallel to the d-axis magnetic circuit at the q-axis to reduce the influence of the magnetic barrier on the L_d. Nevertheless, there is no overload capacity, constant-power speed range, and other indexes directly reflected in the design process. Reasonable control of the magnetization state of PM can improve the efficiency and speed of the motor [16]. In [17]-[19], the comparison of PM magnetization direction and the comparison between segmented and non-segmented PM shows that reasonable control of the magnetization state of PM can improve motor efficiency. In [20], the author analyzes by finite element method that the sinusoidal magnetic density of no-load air gap can be improved by reasonably setting the magnetic barrier along the circumferential direction. At the same time, the low coercivity PM is used in the motor. At low speed, to generate sizeable electromagnetic torque, the PM should be in a state of high magnetization. At high speed, to make the motor have a wider speed range, the PM is in a low magnetization state so that the motor has high efficiency in the whole operating range. In [21] deduces the influence formula of the soft magnetic material area on torque and speed. By optimizing the area of

Manuscript received January 14, 2022; revised February 28, 2022; accepted March 16, 2022. date of publication March 25, 2022; date of current version March 18, 2022.

This work was supported in part by the National Natural Science Foundation of China under Grant 51307045, in part by the Natural Science Foundation of Heilongjiang Province of China under Grant LH2019E075, and in part by the Fundamental Research Funds for the Heilongjiang Province Universities under Grant KJCX201915.

Fei Guo, Qiu Chu, Chunyan Li, and Tao Meng are with the Department of Mechanical and Electrical Engineering, Heilongjiang University, Harbin 150080, China. (e-mail: 2191849@s.hlju.edu.cn; 2202541@s.hlju.edu.cn; lichunyan@hlju.edu.cn; mengtao@hlju.edu.cn.)

(Corresponding Author: Chunyan Li)

Digital Object Identifier 10.30941/CESTEMS.2022.00011.

ferromagnetic materials, the optimum area ratio is obtained. This design avoids the risk of irreversible demagnetization of PM. Due to the low no-load back EMF of the NSPMSM, it can suppress short-circuit current (SCC) without sacrificing overload capacity, which provides a new idea for the fault-tolerant motor to suppress SCC [22]-[25].

This article proposes a W-type NSPMSM with a new rotor structure. The rotor has a simple structure and convenient manufacturing. The W-type permanent magnet can place more permanent magnets and increase the flexibility of permanent magnet design. In section II, the L_d and L_q are obtained by building the equivalent magnetic circuits of the d-axis and q-axis, and the features of the two types of motors are compared. In section III, the motor structure parameters are optimized by analyzing the influence of motor structure on motor performance. In section IV, the performance of the two motors is compared under different internal power factor angles through finite element analysis, and the validity and feasibility of NSPMSM are verified. In section V, the effect of a winding short circuit on the performance of two motors is calculated by studying the characteristics of the motors. Finally, the conclusion is given in section VI.

II. Motor Topology and Operation Principle

A. Motor Topology

Fig. 1 (a) depicts the structure of NSPMSM. The rotor is composed of the iron core, W-type PM, magnetic bridge, and electrode groove. The electrode groove can be rectangular, circular, and another irregular shape. The saliency ratio can be adjusted, and the torque fluctuation can be decreased by setting an appropriately shaped electrode groove in the q-axis. A magnetic bridge is arranged at the electrode groove of the q-axis and the arc of the rotor. The magnetic bridge improves the L_d by providing a path for the d-axis magnetic flux. Although the existence of a magnetic bridge reduces the utilization rate of magnetic flux, the i_d is a flux-intensifying current, which can increase the electromagnetic torque and improve the utilization rate of the motor. This deficiency happens to be transformed into an advantage during the flux-weakening operation, conducive to expanding the motor's wide speed range. The W-type PM forms a magnetic barrier in the q-axis direction to reduce the L_q. The rotor eccentricity leads to the air gap length in the d-axis direction being less than the air gap length in the q-axis direction, which can not only improve the sinusoid of the no-load EMF curve but also implement that the L_d is greater than the L_q. In order to evaluate and study the properties of the NSPMSM, a traditional PSPMSM was designed as a reference under the condition of ensuring the same rated parameters. The PSPMSM structure is presented in Fig. 1 (b).

B. Magnetic Circuit Calculation

The PM is considered as air during the reluctance analysis of the NSPMSM. Fig. 2 shows the flux magnetic distribution of the armature current in the case of only i_d or i_q. When the NSPMSM works normally, the magnetic permeability of stato stator and rotor cores is assumed to be infinite due to the

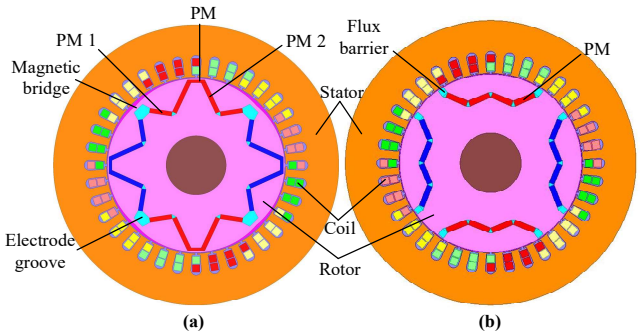

Fig. 1. The topological structure of the motors. (a) NSPMSM. (b) PSPMSM.

unsaturated cores. The air gap in the d-axis magnetic circuit is small, and through the unequal air gap, the d-axis magnetic flux enters the rotor. The permeability of the non-uniform air gap along the d-axis is denoted by $p_{d\delta}$. The d-axis magnetic flux in the rotor is divided into two parts: most of the d-axis magnetic flux flows through the q-axis magnetic bridge, and the rest flows through the PMs. The air gap in the q-axis magnetic circuit is large, and through the unequal air gap, the q-axis magnetic flux enters the rotor. The permeability of the non-uniform air gap along the q-axis is denoted by $p_{q\delta}$. The q-axis magnetic flux in the rotor is divided into two parts: most of the q-axis magnetic flux flows through the PMs, and the rest flows through the d-axis magnetic bridge.

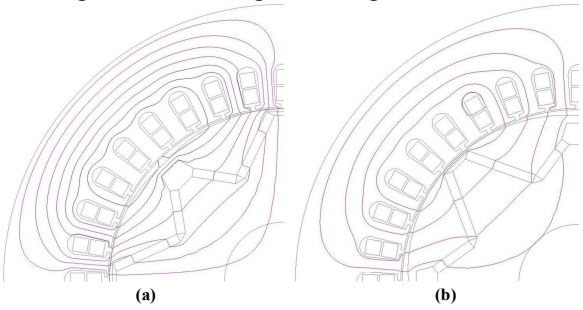

Fig. 2. The magnetic circuit of the NSPMSM. (a) d-axis. (b) q-axis.

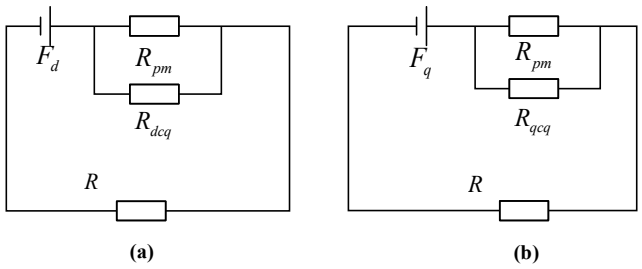

Fig. 3. The equivalent magnetic circuit of the NSPMSM. (a) d-axis. (b) q-axis.

Compared with the q-axis magnetic circuit, the d-axis magnetic circuit with a small air gap can flow into more d-axis magnetic flux. Since there is a magnetic bridge between the electrode groove and the outer circle of the rotor, the permeability of the magnetic bridge is more than the permeability of the PM, and the permeability is denoted as p_m. A large amount of magnetic flux directly passes through the magnetic bridge without passing through the PM, reducing the reluctance of the d-axis magnetic circuit. Meanwhile, due to the special topological structure of the PM, it is difficult for magnetic flux to pass through the q-axis. Thus, the L_d can be

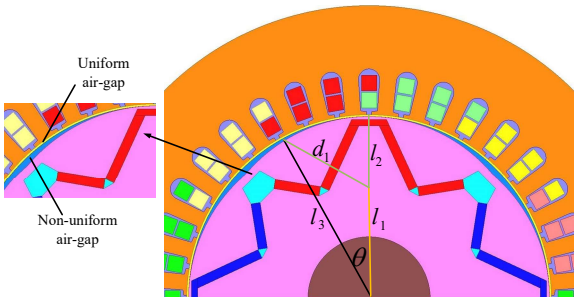

Fig. 4. D-axis magnetic circuit annotation.

greater than the L_q. Fig. 3 shows the equivalent magnetic circuits of the NSPMSM.

As shown in Fig. 4, the d-axis air-gap can be divided into uniform and non-uniform air-gaps. The uniform air-gap permeability $p_{d\delta 1}$ is calculated as follow

$$p_{d\delta 1} = \int_0^{\theta} \frac{\mu_0 l_{ef} l_3 d\theta}{\delta} = \frac{\mu_0 l_{ef} l_3 \theta}{\delta} \tag{1}$$

where μ_0 is the vacuum permeability, δ is the uniform air-gap length, l_{ef} is the motor axial length, and θ and l_3 are shown in Fig. 4.

The uniform air-gap permeability $p_{d\delta 2}$ is calculated as follow

$$p_{d\delta 2} = \int_0^{\theta} \frac{\mu_0 l_{ef} l_3 d\theta}{\sqrt{l_1^2 + l_3^2 - 2 l_1 l_3 \cos\theta} - l_2} \tag{2}$$

where l_1 and l_2 are shown in Fig. 4.

The d-axis air-gap permeability $p_{d\delta}$ is calculated as follow

$$p_{d\delta} = \frac{p_{d\delta 1} p_{d\delta 2}}{p_{d\delta 1} + p_{d\delta 2}} \tag{3}$$

The d-axis magnetic bridge reluctance R_{dcq} is calculated as follow

$$R_{dcq} = \frac{L_k}{\mu_{fe} h_{cq} L_{ef}} \tag{4}$$

where h_{cq} and L_k are the radial height and horizontal width of the magnetic bridge respectively. μ_{fe} is the core permeability.

The total magnetic permeability p_{dM} at each pole PM is formed by PM and the magnetic bridge between the rotor and the electrode groove in parallel. p_{dM} is given by (5)

$$P_{dM} = \frac{\mu_0 l_{ef} b_M}{h_M} + \frac{1}{R_{dcq}} \tag{5}$$

The L_d is calculated as follow

$$L_d = N^2 \frac{p_{dM} p_{d\delta}}{(p_{dM} + p_{d\delta})} \tag{6}$$

The q-axis air-gap can be divided into uniform air-gap and non-uniform air-gap, as shown in Fig. 5.

The uniform air-gap permeability $p_{q\delta 1}$ is calculated as follow

$$p_{q\delta 1} = \int_0^{\beta} \frac{\mu_0 l_{ef} l_6 d\alpha}{\delta} = \frac{\mu_0 l_{ef} l_6 \beta}{\delta} \tag{7}$$

where β is shown in Fig. 5.

The non-uniform air-gap permeability $p_{q\delta 2}$ is calculated as follow

$$p_{q\delta 2} = \int_0^{\beta} \frac{\mu_0 l_{ef} l_3 d\beta}{\sqrt{l_4^2 + l_6^2 - 2 l_4 l_6 \cos\alpha} - l_5} \tag{8}$$

where l_4, l_5, and l_6 are shown in Fig. 5.

The q-axis air-gap permeability $p_{q\delta}$ is calculated as follow

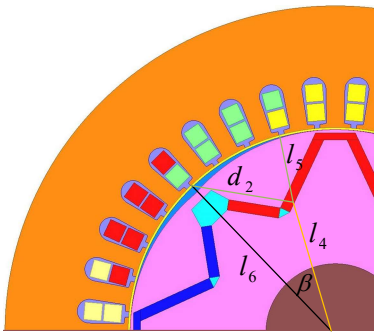

Fig. 5. Q-axis magnetic circuit annotation.

$$p_{q\delta} = \frac{p_{q\delta 1} p_{q\delta 2}}{p_{q\delta 1} + p_{q\delta 2}} \tag{9}$$

The q-axis magnetic bridge reluctance R_{qcq} is calculated as follow

$$R_{qcq} = \frac{L_k}{\mu_{fe} h_{cq} L_{ef}} \tag{10}$$

The total magnetic permeability p_{qM} at each pole PM is formed by PM and the magnetic bridge between the rotor and the electrode groove in parallel. p_{qM} is given by (11)

$$P_{qM} = \frac{\mu_0 l_{ef} b_M}{h_M} + \frac{1}{R_{qcq}} \tag{11}$$

The L_q is calculated as follow

$$L_q = N^2 \frac{p_{qM} p_{q\delta}}{(p_{qM} + p_{q\delta})} \tag{12}$$

The following relationship is obtained when L_d is greater than L_q.

$$N^2 \frac{p_{dM} p_{d\delta}}{(p_{dM} + p_{d\delta})} > N^2 \frac{p_{qM} p_{q\delta}}{(q_{qM} + p_{q\delta})} \tag{13}$$

According to the above formula, L_d and L_q depend on magnetic bridge width, the PM width, and non-uniform air-gap size. Parameters of the NSPMSM should meet Equation (13). Since the magnetic bridge width in the d-axis path is greater than the magnetic bridge width in the q-axis path, and the d-axis air-gap length is less than the q-axis air-gap length, the L_d is greater than the L_q.

C. *Negative-salient Pole Feature*

In order to verify that the negative-salient pole feature can be realized in the new motor structure, under the condition of equivalent d-axis current or q-axis current, the magnetic field lines and magnetic flux density distributions of the d-axis and q-axis are investigated using the finite element method, as shown in Fig. 6. Under the condition of the same q-axis current or d-axis current, the d-axis magnetic field lines are significantly denser than the q-axis magnetic field lines, and the d-axis magnetic flux density is significantly denser than the q-axis magnetic flux density. It is sufficient to verify that the L_d is larger than the L_q. In addition, the NSPMSM provides a path for d-axis magnetic flux through structural innovation. As can be seen from the magnetic flux density distribution, the magnetic flux of the NSPMSM mainly passes through the magnetic bridge. Therefore, the irreversible demagnetization

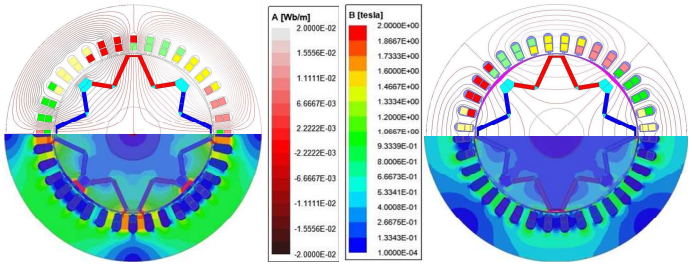

Fig. 6. The distribution of d-axis and q-axis magnetic field lines and magnetic flux density of the NSPMSM. (a) d-axis. (b) q-axis.

problem is caused by the flux-weakening current can be improved.

D. Torque Angle Characteristics of the NSPMSM

The electromagnetic torque of PMSM with salient pole effect is given by (14)

$$T_{em} = m\frac{E_0 U}{X_d \Omega_s}\sin\theta + m\frac{U^2}{2\Omega_s}\left(\frac{1}{X_q}-\frac{1}{X_d}\right)\sin 2\theta \quad (14)$$

where U is the power supply voltage, m is the number of phases, E_0 is no-load back EMF, Ω_s is the synchronous angular velocity, θ is the torque angle, X_d and X_q are d-axis and q-axis reactance respectively.

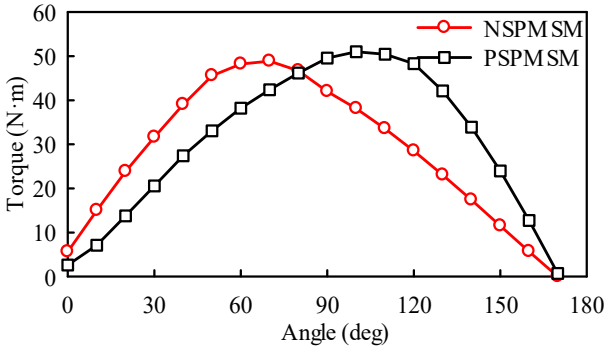

Fig. 7. Torque angle characteristics of two kinds of PMSMs.

When rated load voltage is applied to the NSPMSM and PSPMSM, the power angle corresponding to the average value of maximum electromagnetic torque obtained under different power angles is shown in Fig. 7 through parametric scanning of finite element software. Different from the PSPMSM, the maximum torque angle of the NSPMSM is less than 90 degrees. Therefore, the reluctance torque component of the NSPMSM is positive when the torque angle is less than 90 degrees, which again indirectly indicates that the L_d is greater than the L_q. When the NSPMSM works under rated load, the direction of the d-axis armature MMF is the same as the PM MMF, which can increase the electromagnetic torque and improve the utilization rate of the PM, thus enhancing the stability of PM during the operation of the motor.

III. Influence of Motor Structure on Performance of the NSPMSM

A. Influence of PM on Inductance

The saliency ratio ρ can be used to describe the relationship between L_d and L_q.

$$\rho = \frac{L_d}{L_q} \quad (15)$$

Fig. 8 shows the changes of L_d and L_q of the PSPMSM with the thickness of PM when only the thickness of the PM is changed with the same size of other parameters. The L_d decreases with the increase of the thickness of the PM, but with the increase of the thickness, the d-axis magnetic circuit is gradually saturated. The thickness of the PM has little effect on the L_q. Fig. 8 shows that the L_q is greater than L_d.

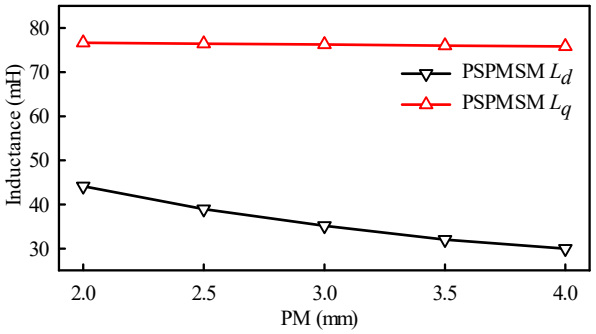

Fig. 8. Influence of PM thickness on L_d and L_q of the PSPMSM. (a) L_d. (b) L_q.

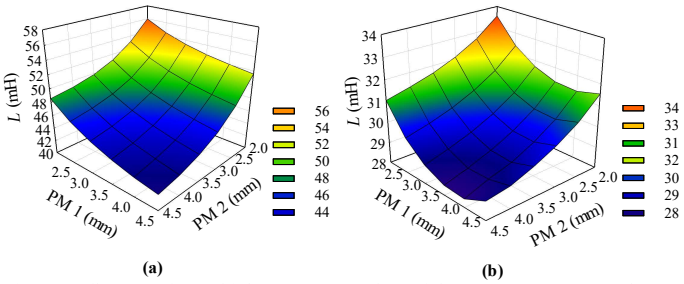

Fig. 9. Influence of PM thickness on L_d and L_q of the NSPMSM. (a) L_d. (b) L_q.

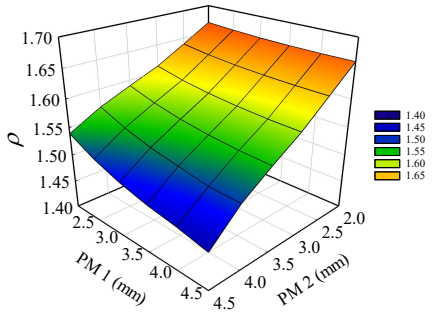

Fig. 10. Influence of PM thickness on salient pole ratio of the NSPMSM.

It can be witnessed from Fig. 9 and Fig. 10 that the increase of the PM thickness decreases the L_d and the L_q, but the thickness of PM 2 has a relatively significant impact on the L_d, and the decrease of PM 2 is more conducive to the improvement of the L_d. The L_q is not only affected by the structure variation of the d-axis but also affected by the saturation of the d-axis magnetic circuit.

Fig. 11 shows the change of average magnetic flux density with the thickness of PM, and the influence of the PM thickness on the torque and speed is shown in Fig. 12. Increasing the thickness of the PM will make the PM provide more PM magnetic flux, which improves the electromagnetic torque. However, increasing the size to a certain value will cause motor saturation. As the thickness of PM increases, the maximum speed of the motor decreases. Therefore, the thickness of PM

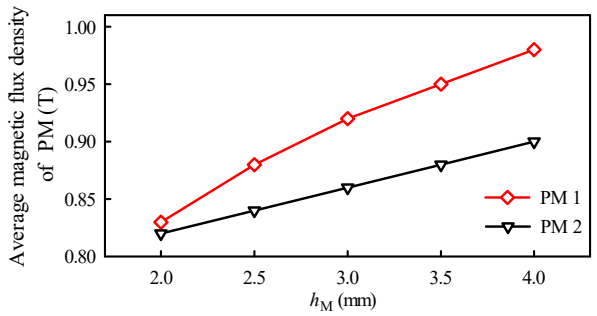

Fig. 11. The average magnetic flux density of the PM varies with h_M.

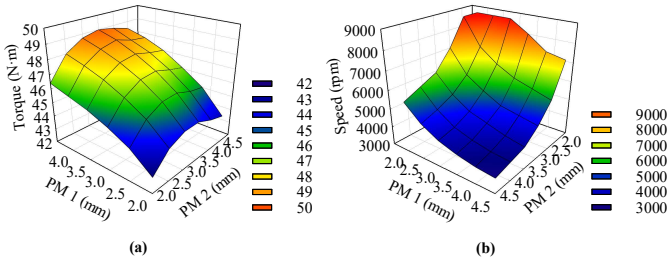

Fig. 12. Influence of PM thickness on torque and speed of the NSPMSM. (a) torque. (b) speed.

can be selected as the thinnest size under electromagnetic torque conditions. The PM thickness of the NSPMSM is finally set as 3mm.

B. Influence of Rotor Eccentricity on the NSPMSM

The air-gap magnetic flux density can be improved by increasing the eccentricity of the rotor. The deviation distance s is defined as the difference between the furthest distance from the center of the circle in the d-axis and the furthest distance from the center of the circle in the q-axis. The different eccentricity reflects the circular arc degree of the outer core of the rotor and represents the degree of the unequal air gap. Finite element software is used to investigate the impact of various eccentric distances on the air gap, as shown in Fig. 13 and Fig. 14. The sinusoidal waveform of the air gap magnetic flux density can be improved by moderate rotor eccentricity. However, if the eccentricity distance is too large, the higher harmonic content of the air gap magnetic flux density waveform will increase obviously. It has a certain influence on motor loss and vibration.

Rotor eccentricity improves the sinusoidal density of the air gap and affects the electromagnetic torque and motor speed. As shown in Fig. 15, finite element software is applied to calculate the influence of different eccentric distances on torque and speed. With the increase of eccentricity distance, the equivalent

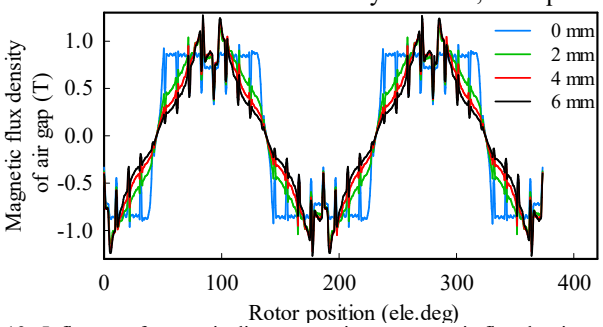

Fig. 13. Influence of eccentric distance on air-gap magnetic flux density of the motors.

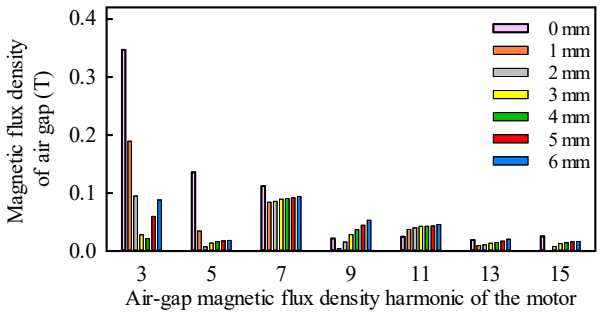

Fig. 14. Influence of eccentric distance on air-gap magnetic flux density harmonics of the motors.

air-gap length increases, leading to the increase of magnetoresistance of the primary magnetic circuit, and the electromagnetic torque decreases as the air-gap magnetic flux density decreases. The decrease of air-gap magnetic flux density is beneficial to enlarge the speed range. When selecting eccentric distance, a relatively sizeable eccentric distance value should be selected on the premise of satisfying the rated torque to increase the flux-weakening range of the NSPMSM.

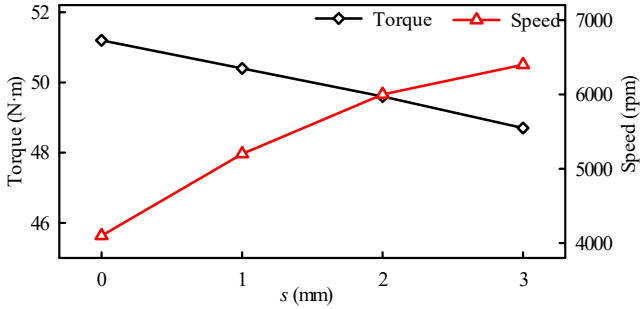

Fig. 15. Influence of rotor eccentricity on torque and speed.

C. Influence of Magnetic Bridge on the NSPMSM

The width d of the magnetic bridge between the electrode groove at the q-axis and the outer circle of the rotor affects the performance of the NSPMSM. The width of the magnetic bridge can be regulated by adjusting the shape and size of the electrode groove. As shown in Fig. 16, the influence of different magnetic bridge widths on the inductance is calculated by using finite element software. The influence of electromagnetic torque and speed is presented in Fig. 17.

As the magnetic bridge becomes broad, the more magnetic field lines closed by the PM through the magnetic bridge inside the rotor, the leakage flux will be greater. With the rise in the breadth of the magnetic bridge, the electromagnetic torque gradually decreases. The width of the magnetic bridge affects

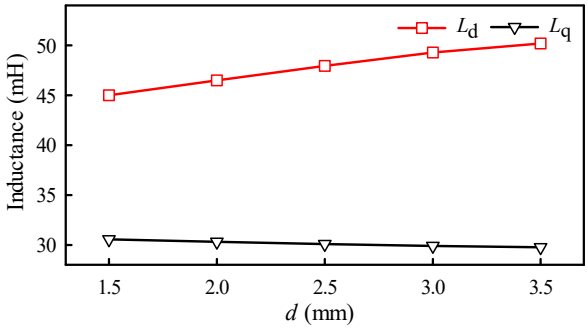

Fig. 16. Influence of magnetic bridge on inductance.

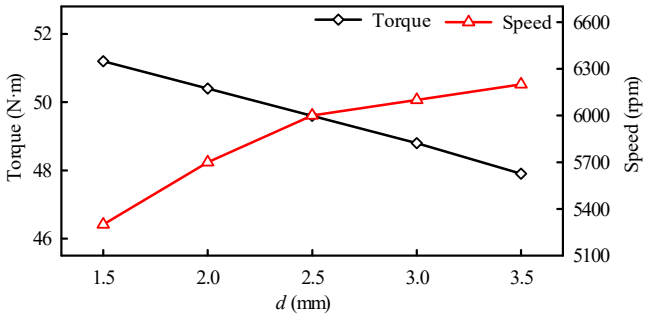

Fig. 17. Influence of magnetic bridge on torque and speed.

the inductance of the NSPMSM and the motor speed range. The maximum speed increases with the increase of magnetic bridge width, but the maximum speed increases slowly. When selecting magnetic bridge width, the maximum value should be selected on the premise of satisfying the electromagnetic torque to improve the flux-weakening range. Table 1 shows the parameters of the NSPMSM and PSPMSM.

TABLE I
THE PARAMETERS OF THE NSPMSM AND PSPMSM

Parameters	NSPMSM	PSPMSM
Stator outer diameter	190mm	190mm
Stator inner diameter	120mm	120mm
Air-gap length	0.6mm	0.6mm
Axial length	100mm	100mm
h_M	3mm	3.5mm
Rated speed	1500rpm	1500rpm
Rated power	7.5kW	7.5kW
Rated voltage	380V	380V

IV. INFLUENCE OF THE INTERNAL POWER FACTOR ANGLE ON MOTOR

When the two motors run under the control of maximum torque per ampere (MTPA), the i_d is flux-intensifying current or flux-weakening current respectively. ψ is the angle between the no-load back EMF and the armature currents. It is defined as negative when the no-load back EMF lags behind the armature current phase.

A. Influence of the Internal Power Factor Angle on Torque and Speed of the Motor

The current vector trajectory of the NSPMSM is shown in Fig. 18, and its maximum torque-current curve is located in the first quadrant. When $0<\omega<\omega_1$ (ω is the rated speed), the current vector trajectory is located in the first quadrant, and i_d is the flux-intensifying current; When $\omega_1<\omega<\omega_2$, the current vector trajectory gradually moves from the first quadrant to i_q, and i_d transitions from the magnetization state to the critical state of neither magnetization nor demagnetization. When $\omega>\omega_2$, the current vector trajectory is located in the second quadrant, and i_d is the flux- weakening current. It can be witnessed that in most working states of the NSPMSM, the d-axis armature reaction is flux-intensifying current.

When the NSPMSM uses the flux-weakening control method, the linear velocity is given by (16).

$$n = \frac{60u_{\lim}}{2\pi\sqrt{\left(L_d i_d\right)^2 + \left(L_d i_d + \psi_f\right)^2}} \tag{16}$$

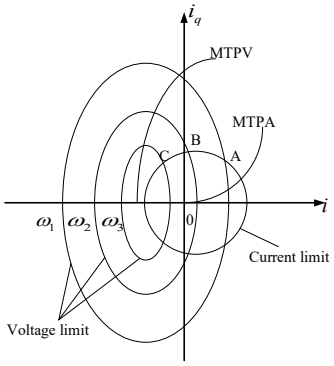

Fig. 18. Current vector trajectory diagram of the NSPMSM.

where u_{lim} is the limit voltage of the motor.

When the voltage and current at the motor end reach the maximum value, the ideal maximum speed that the motor can achieve is given by (17).

$$n_{\max} = \frac{60u_{\lim}}{2\pi p\left|\psi_f - L_d i_{\lim}\right|} \tag{17}$$

where i_{lim} is the limit current of the motor.

The maximum speed of a motor is primarily determined by the PM flux linkage and L_d when the limiting voltage and limiting current are constant. Smaller PM linkage flux and larger L_q are beneficial to enlarge the flux-weakening range. When the ratio of PM flux linkage to L_d is equal to the limit current, theoretically the motor can run at any speed. Due to the existence of armature magnetomotive force harmonics and no-load back EMF harmonics, the constant-power speed range cannot be infinite even if the characteristic current is equal to the limit current.

The electromagnetic torque of the motor is not only related to the current but also related to the internal power factor angle. Fig. 19 depicts how the internal power factor angle varies with the speed of NSPMSM and PSPMSM. When the NSPMSM operates at or below the rated speed, ψ is positive, reducing the risk of PM's irreversible demagnetization. When the PSPMSM operates at full speed, ψ is always negative. Fig. 20 presents the relationship between the d-axis current, q-axis current, and speed of NSPMSM and PSPMSM. Since the salient ratio of the NSPMSM is greater than 1, in the low-speed operation area, the NSPMSM only requires a small positive i_d to generate positive reluctance torque, and the motor needs a large i_q to generate permanent magnet torque under MTPA control.

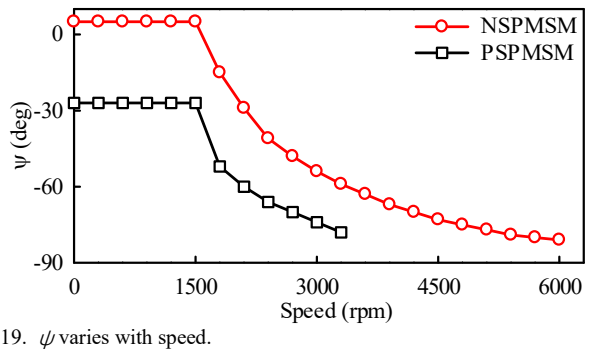

Fig. 19. ψ varies with speed.

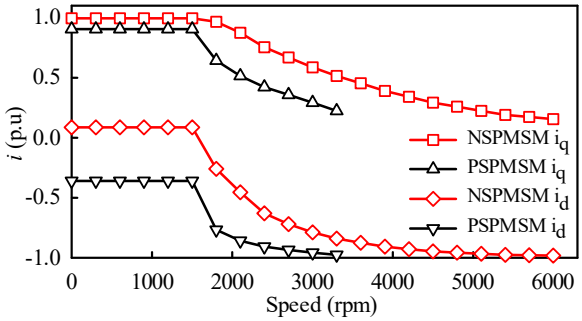

Fig. 20. Relationship between motor current and speed.

In the low-speed region, The NSPMSM operates under the condition of small i_d, hence, the proportion of reluctance torque is less than the proportion of the PSPMSM. However, the large reluctance torque obtained in the PSPMSM will also bring a high risk of irreversible demagnetization of PM. In the high-speed region, the increase of L_d results in the amplitude of flux-weakening current required by the NSPMSM being less than the amplitude of flux-weakening current of the PSPMSM. The risk of irreversible demagnetization of NSPMSM is greatly reduced.

Fig. 21 depicts the torque-speed curves of the NSPMSM and PSPMSM. The output torque of the PSPMSM is higher than the output torque of the NSPMSM in the low-speed operation area. In the high-speed operation zone, the maximum speed of the PSPMSM can only reach 3300 rpm. Due to the large L_d of the NSPMSM, when the electromagnetic torque of the motor exactly neutralizes the no-load friction torque, the rotational speed of the NSPMSM reaches its limit. The friction torque is approximately 2 N·m calculated by electromagnetic torque of 4%. As can be witnessed from Fig. 21, when the NSPMSM runs at 6000 rpm, the output torque of the motor can overcome the no-load friction torque, and the effective value of the electrodynamic force of the motor load phase is lower than 220 V, which means the NSPMSM can be expanded to at least 6000 r/min. Fig. 22 depicts the power-speed curves of the NSPMSM and PSPMSM. In the low-speed operating region, the power of the NSPMSM is slightly less than the power of the PSPMSM. In the high-speed operating state, The NSPMSM operates at a smaller flux-weakening current, thus reducing the risk of irreversible demagnetization of NSPMSM and widening the constant-power speed range of the motor in a flux-weakening state.

B. Influence of the Internal Power Factor Angle on Risk of Irreversible Demagnetization of PM

The material of PM used in two motors is NdFe35. Fig. 23

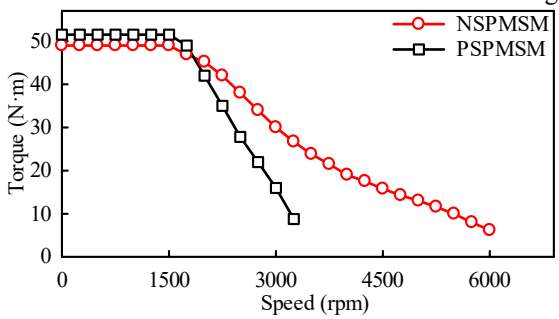

Fig. 21. Torque-speed curves of two motors.

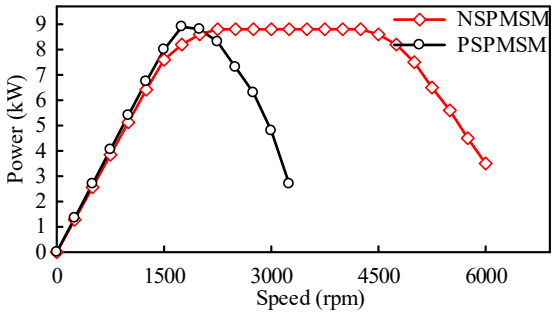

Fig. 22. Power-speed curves of two motors.

shows the running track of the PM of the NSPMSM and the PSPMSM. The demagnetization curve of NdFe35 is a straight line at room temperature, and it coincides with a recoil line. The demagnetization curve of the PM exhibits a knee point when the temperature is greater than 120°C. The magnetic flux density at the inflection point is 0.17 T. When the magnetic flux density of the PM falls below the knee point, it is irreversibly demagnetized.

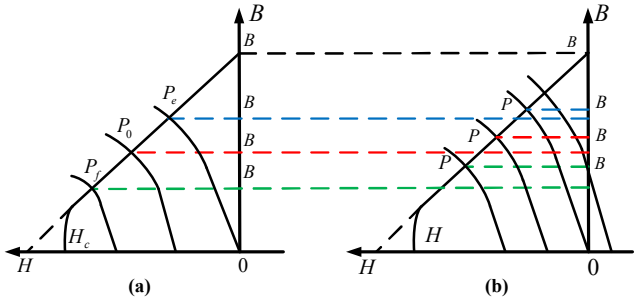

Fig. 23. Torque-speed curves of two motors.

B_0 is the working point of the PM corresponding to main relative permeability P_0 under the no-load condition, B_e is the working point of the PM corresponding to main relative permeability P_e under the rated current, B_f is the working point of the PM corresponding to the main relative permeability P_f under the flux-weakening current. When ψ is greater than 0, the motor runs in the low-speed region. The motor is operating in the flux-intensifying state, and the required current is positive i_d. At this time, the operation point of the PM of the motor will move from P_0 to P_e. The working point of the PM at P_e is much higher than the knee point of the PM, and the risk of irreversible demagnetization of the PM is relatively low. When ψ is less than 0, the NSPMSM is operating in the flux-weakening state. The required current is negative i_d, and the working point of the PM will move from P_0 to P_f. Due to the special inductance characteristics of the NSPMSM, only a small flux-weakening current is required when the NSPMSM is operating in the flux-weakening state. As a result, the working point of the PM at P_f is much higher than the knee point, thus reducing the risk of irreversible demagnetization.

Fig. 24 and Fig. 25 show the magnetic density distribution of the motor. The magnetic density of PM of the PSPMSM is 0.66 T at 3300 rpm. At a speed of 6000rpm, the magnetic density at point A of PM is 0.3 T, and the magnetic flux density of the other PM is 0.6 T. It means that the irreversible demagnetization risk of NSPMSM is low under the condition of

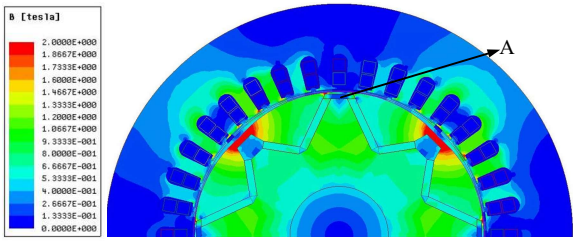

Fig. 24. Magnetic flux density distribution of the NSPMSM at 6000 rpm.

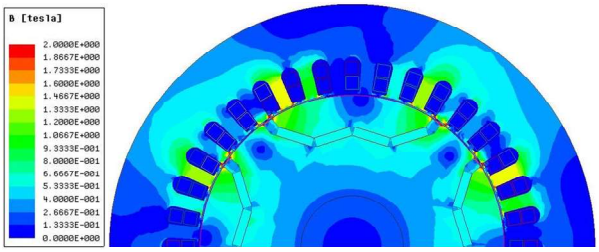

Fig. 25. Magnetic flux density distribution of the PSPMSM at 3300 rpm.

deep flux-weaking state. Based on the above analysis, it can be known that the NSPMSM can maintain a high PM operating point in both the flux-intensifying and the flux-weakening state to avoid irreversible demagnetization of PM effectively.

V. Influence of Winding Short Circuit on the NSPMSM

When winding is short-circuited, the SCC is frequently greater than the rated current. When a short circuit occurs at the end of the winding, the end voltage is 0, so the voltage equation when the fault occurs is shown in equations (18) and (19). The SCC can be suppressed by decreasing the no-load back EMF and increasing the impedance. The phasor diagram of the stable operation of the two is shown in Fig. 26.

$$0 = L\frac{di}{dt} + e + R_1 i \tag{18}$$

$$i = \frac{E_0}{\sqrt{(2\pi fL)^2 + R_1^2}} \tag{19}$$

where i is the SCC, L is the winding inductance, t is the time, e is the induction electromotive force, R_1 is the winding resistance, f is the frequency, E_0 is the no-load back EMF.

In Fig. 26, X_1 is the stator leakage reactance; E_{0+} and E_{0-} are no-load back EMF of the NSPMSM and the PSPMSM respectively. When the terminal voltage of PSPMSM is the same as the terminal voltage of NSPMSM, the no-load back EMF of NSPMSM is lower. Therefore, the NSPMSM has more vital SCC suppression ability, and it is not easy to produce feedback generation phenomenon in the flux-weakening state, which improves the reliability of the motor and its control system.

Fig. 27 and Fig. 28 show the SCC and torque changes when the winding of the NSPMSM and the PSPMSM short-circuit, where T is the period of the motor. The steady-state SCC is 1.1 and 1.35 times the rated current, respectively. The steady-state torque fluctuation of the PSPMSM is fewer. When the NSPMSM and PSPMSM have the same impedance, the NSPMSM has a high SCC suppression ability.

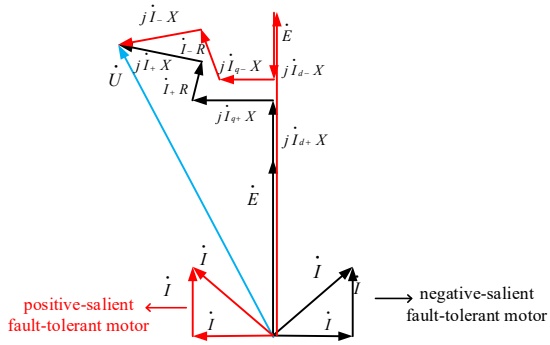

Fig. 26. Phasor diagram of NSPMSM and PSPMSM.

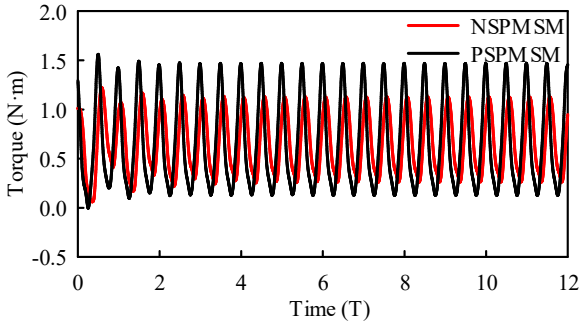

Fig. 27. Torque of the PMSMs when the winding terminal is short-circuited.

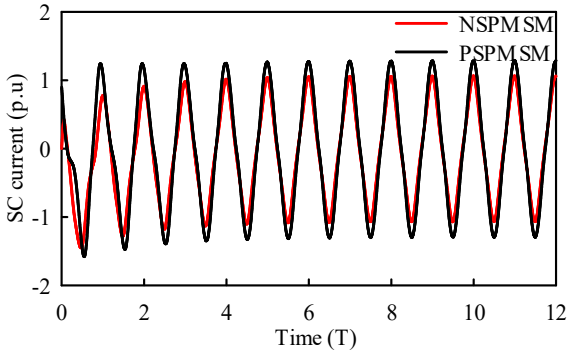

Fig. 28. Terminal SC Current of the PMSMs.

VI. Conclusion

This article designed a W-type NSPMSM with a particular rotor structure based on the equivalent magnetic circuit and finite element analysis. Through qualitative analysis and quantitative calculation, it is shown that the i_d is greater than 0 when the base speed and below is running, and the flux-intensifying current avoids the risk of irreversible de-magnetization of the PM. In the range of the motor's full speed, the i_d transits from flux-intensifying current to flux-weakening current, and the wide adjustment range of current angle is conducive to broadening the range of constant-power speed regulation. When the inverter capacity is fixed, its i_q is more extensive, conducive to maintaining permanent magnet torque and power during speed regulation. When the winding of the NSPMSM is short-circuiting, the SCC can be suppressed without sacrificing the overload capacity, indicating that the NSPMSM has strong SCC suppression capability, which provides a new idea for the fault-tolerant motor. The electrode groove results in more significant leakage flux than a PSPMSM and the utilization rate of a PM decreases

slightly, but it can still meet the rated power output through simulation calculation. This disadvantage is transformed into an advantage in the flux-weakening state, which helps to widen the motor's flux-weakening range. This scheme offers a new approach to solving the flux-weakening problem of PMSM and has theoretical and practical value.

REFERENCES

[1] X. Zhou, X. Zhu, W. Wu, Z. Xiang, Y. Liu and L. Quan, "Multi-objective Optimization Design of Variable-Saliency-Ratio PM Motor Considering Driving Cycles," *IEEE Trans. Ind. Electron.*, vol. 68, no. 8, pp. 6516-6526, Aug. 2021.

[2] D. Ngo, M. Hsieh and T. A. Huynh, "Torque Enhancement for a Novel Flux Intensifying PMa-SynRM Using Surface-Inset Permanent Magnet," *IEEE Trans. Magn.*, vol. 55, no. 7, pp. 1-8, July 2019, Art no. 8106108.

[3] W. Tong, R. Sun, C. Zhang, S. Wu and R. Tang, "Loss and Thermal Analysis of a High-Speed Surface-Mounted PMSM With Amorphous Metal Stator Core and Titanium Alloy Rotor Sleeve," *IEEE Trans. Magn.*, vol. 55, no. 6, pp. 1-4, June 2019, Art no. 8102104.

[4] X. Tang, X. Wang, G. Li and M. Tian, "Demagnetization Study of Line-start Permanent Magnet Synchronous Motor Under Out-of-step and Supersynchronous faults," *in Proc. IEEE Conf. Ind. Electron. Appl. (ICIEA)*, Hefei, China, 2016, pp. 1496-1501.

[5] Y. Chen, Y. Wang, Y. Shen and R. Tang, "Magnetic Circuit Design and Finite Element Analysis of Wide-speed Controllable-Flux PMSM," *Proceedings of the CSEE*, vol. 25, no.20, pp. 157-161, 2005.

[6] T. Wang, X. Zhu, S. Zheng, L. Quan, Z. Xiang and X. Zhou, "Investigation on Torque Characteristic and PM Operation Point of Flux-Intensifying PM Motor Considering Low-Speed Operation," *IEEE Trans. Magn.*, vol. 57, no. 2, pp. 1-5, Feb. 2021, Art no. 8102005.

[7] X. Zhu, W. Wu, S. Yang, Z. Xiang and L. Quan, "Comparative Design and Analysis of New Type of Flux-Intensifying Interior Permanent Magnet Motors With Different Q-Axis Rotor Flux Barriers," *IEEE Trans. Energy Convers.*, vol. 33, no. 4, pp. 2260-2269, Dec. 2018.

[8] Y. Hu, Y. Li, X. Ma, X. Li and S. Huang, "Flux-Weakening Control of Dual Three-Phase PMSM Based on Vector Space Decomposition Control," *IEEE Trans. Power Electron.*, vol. 36, no. 7, pp. 8428-8438, July 2021.

[9] W. Li, K. T. Chau, Y. Gong, J. Z. Jiang and F. Li, "A New Flux-Mnemonic Dual-Magnet Brushless Machine," *IEEE Trans. Magn.*, vol. 47, no. 10, pp. 4223-4226, Oct. 2011.

[10] B. Stumberger, A. Hamler, M. Trlep and M. Jesenik, "Analysis of interior permanent magnet synchronous motor designed for flux weakening operation," *IEEE Trans. Magn.*, vol. 37, no. 5, pp. 3644-3647, Sept. 2001.

[11] T. A. Huynh and M. Hsieh, "Irreversible Demagnetization Analysis for Multilayer Magnets of Permanent Magnet-Assisted Synchronous Reluctance Machines Considering Current Phase Angle," *IEEE Trans. Magn*, vol. 55, no. 7, pp. 1-9, July 2019, Art no. 8106609.

[12] D. Fernández, M. Martínez, D. Reigosa, J. M. Guerrero, C. M. Suárez Alvarez and F. Briz, "Impact of Machine Magnetization State on Permanent Magnet Losses in Permanent Magnet Synchronous Machines," *IEEE Trans. Ind. Appl.*, vol. 55, no. 1, pp. 344-353, Jan.-Feb. 2019.

[13] X. Zhao, B. Kou, L. Zhang and H. Zhang, "Design and Analysis of Permanent Magnets in a Negative-Salient Permanent Magnet Synchronous Motor," *IEEE Access*, vol. 8, pp. 182249-182259, 2020.

[14] X. Zhu, J. Huang, L. Quan, Z. Xiang and B. Shi, "Comprehensive Sensitivity Analysis and Multiobjective Optimization Research of Permanent Magnet Flux-Intensifying Motors," *IEEE Trans. Ind. Electron.*, vol. 66, no. 4, pp. 2613-2627, April 2019.

[15] X. Zhu, S. Yang, Y. Du, Z. Xiang and L. Xu, "Electromagnetic Performance Analysis and Verification of a New Flux-Intensifying Permanent Magnet Brushless Motor With Two-Layer Segmented Permanent Magnets," *IEEE Trans. Magn.*, vol. 52, no. 7, pp. 1-4, July 2016, Art no. 8204004.

[16] A. Fatemi, D. M. Ionel, N. A. O. Demerdash, D. A. Staton, R. Wrobel and Y. C. Chong, "Computationally Efficient Strand Eddy Current Loss Calculation in Electric Machines," *IEEE Trans. Ind. Appl.*, vol. 55, no. 4, pp. 3479-3489, July-Aug. 2019.

[17] N. Limsuwan, T. Kato, K. Akatsu and R. D. Lorenz, "Design and Evaluation of a Variable-Flux Flux-Intensifying Interior Permanent-Magnet Machine," *IEEE Trans. Ind. Appl.*, vol. 50, no. 2, pp. 1015-1024, March-April 2014.

[18] T. Kato, N. Limsuwan, C. Yu, K. Akatsu and R. D. Lorenz, "Rare Earth Reduction Using a Novel Variable Magnetomotive Force Flux-Intensified IPM Machine," *IEEE Trans. Ind. Appl.*, vol. 50, no. 3, pp. 1748-1756, May-June 2014.

[19] T. Fukushige, N. Limsuwan, T. Kato, K. Akatsu and R. D. Lorenz, "Efficiency Contours and Loss Minimization Over a Driving Cycle of a Variable Flux-Intensifying Machine," *IEEE Trans. Ind. Appl.*, vol. 51, no. 4, pp. 2984-2989, July-Aug. 2015.

[20] M. Ibrahim, L. Masisi and P. Pillay, "Design of Variable Flux Permanent-Magnet Machine for Reduced Inverter Rating," *IEEE Trans. Ind. Appl.*, vol. 51, no. 5, pp. 3666-3674, Sept.-Oct. 2015.

[21] R. H. Moncada, J. A. Tapia and T. M. Jahns, "Analysis of Negative-Saliency Permanent-Magnet Machines," *IEEE Trans. Ind. Electron.*, vol. 57, no. 1, pp. 122-127, Jan. 2010.

[22] W. Zhang, X. Liang and F. Yu, "Fault-Tolerant Control of Hybrid Excitation Axial Field Flux-Switching Permanent Magnet Machines," *IEEE Trans. Magn.*, vol. 54, no. 11, pp. 1-5, Nov. 2018, Art no. 8106305.

[23] X. Jiang, D. Xu, L. Gu, Q. Li, B. Xu and Y. Li, "Short-Circuit Fault-Tolerant Operation of Dual-Winding Permanent-Magnet Motor Under the Four-Quadrant Condition," *IEEE Trans. Ind. Electron.*, vol. 66, no. 9, pp. 6789-6798, Sept. 2019.

[24] G. Liu, C. Song and Q. Chen, "FCS-MPC-Based Fault-Tolerant Control of Five-Phase IPMSM for MTPA Operation," *IEEE Trans. Power Electron.*, vol. 35, no. 3, pp. 2882-2894, March 2020.

[25] N. Pothi, Z. Q. Zhu and Y. Ren, "Comparison of Flux-Weakening Control Strategies of Novel Hybrid-Excited Doubly Salient Synchronous Machines," *IEEE Trans. Ind. Appl.*, vol. 55, no. 4, pp. 3589-3597, July-Aug. 2019.

FEI GUO was born in Shanxi Province, China, in 1994. He received the B.S. degree in Electrical Engineering from Heilongjiang University, Harbin, China, in 2018.

He is currently pursuing the M.S. degree in Electrical Engineering with Heilongjiang University, Harbin, China. His research interest includes the design and control of negative-salient permanent magnet synchronous motor.

QIU CHU was born in Jilin Province, China, in 1994. She received the B.S. degree in automation from Jilin Engineering Normal University, Jilin, China, in 2015.

She is currently pursuing the M.S. degree in Electrical Engineering from Heilongjiang University, Harbin, China. Her research interest include the design and control of Halbach permanent magnet synchronous motors.

CHUNYAN LI was born in Heilongjiang Province, China, in 1980. She received the B.S. degree in Automation from Heilongjiang University, Harbin, China, in 2003, and the M.S., and Ph.D. degrees in Electrical Engineering from the Harbin Institute of Technology, Harbin, China, in 2005 and 2010, respectively.

She is currently an Associate Professor with the School of Mechanical and Electrical Engineering, Heilongjiang University. Her research interests include the design and control of permanent magnet synchronous motors.

TAO MENG was born in Liaoning Province, China, in 1980. He received the B.S., M.S., and Ph.D. degrees in Electrical Engineering from the Harbin Institute of Technology, Harbin, China, in 2003, 2005, and 2010, respectively.

He is currently a Professor with the School of Mechanical and Electrical Engineering, Heilongjiang University. His research interests include high frequency and dc/dc conversion, and high-frequency magnetic devices.